Struct Chem (2012) 23:1369–1375
DOI 10.1007/s11224-012-0056-5

ORIGINAL RESEARCH

# On the asymmetry in molybdenum–oxygen bonding in the $MoO_3$ structure: ETS–NOCV analysis

**Mariusz P. Mitoraj · Artur Michalak**

Received: 14 July 2011 / Accepted: 17 March 2012 / Published online: 4 June 2012


**Abstract** In the present study, the analysis of *natural orbitals for chemical valence* (NOCV) combined with the *extended-transition-state* (ETS) bond-energy decomposition method (ETS–NOCV) was applied to characterize an asymmetry in Mo–O bonding in $MoO_3$ crystal. Considered were three non-equivalent oxygen sites (O1, O2, O3) in the $Mo_7O_{30}H_{18}$ cluster model of (010) surface of $MoO_3$. The ETS–NOCV method leads to the conclusion that an increase in the Mo–O distances, from 1.68 Å (for Mo–O1), through 1.73 Å (for Mo–O2), up to 1.94 Å (for Mo–O3), is directly related to decrease in strength of both $\sigma$- and $\pi$-contributions of Mo–O bond. Further, Mo–O connection appeared to exhibit both ionic (the charge transfer from 2*p* orbital of oxygen to molybdenum) and the covalent (charge accumulation in the region of Mo–O) components. Finally, the trend in the orbital energy stabilization ($\Delta E_{orb}$) originating from the dominant $\sigma$- and $\pi$-bond contributions appeared to correlate very well with the oxygen-vacancy formation energies published earlier by Tokarz-Sobieraj et al. (Surf Sci 489:107, 2001).

**Keywords** Molybdenum oxide · Charge and energy decomposition · ETS-NOCV · NOCV-deformation density contributions

## Introduction

Since the pioneering applications of theoretical methods of quantum-chemistry in heterogeneous catalysis, [1–6] the computational approaches based on both, cluster models and periodic approaches, provide nowadays standard tools for investigating the properties of the active sites of catalysts and the mechanisms of catalytic reaction. Among many examples in catalysis, the theoretical investigations on the structural and electronic surface properties and the catalytic reactions of transition-metal oxides, in particular based on vanadium and molybdenum, [7–21] are especially important as they provided a deep insight into the structure–activity relationship of these compounds, used in a variety of applications.

Besides its importance in catalysis, [22, 23] the molybdenum oxide $MoO_3$ provides an interesting example of chemical bonding, because of the existence in its crystal structure [24] of three non-equivalent oxygen atoms, leading to molybdenum–oxygen bonds of different character. Namely, the ionic, layer type orthorhombic structure of $MoO_3$ is built of the distorted $MoO_3$ octahedra sharing the oxygen atoms, and the (010) surface represents the easy cleavage plane of the crystal. The features of the $MoO_3$ structure are visualized in Fig. 1 using the example of the $Mo_7O_{30}H_{18}$ cluster modeling of the (010) surface. The O1 oxygen atom is bound to molybdenum atom by the shortest bond (1.67 Å). The O2 site (and the equivalent O2′) is linked to one molybdenum atom by the relatively short bond (1.73 Å), and is substantially more distant from another metal atom (2.25 Å). The third oxygen type O3 (and O3′, O3″) is bound symmetrically to two molybdenum atoms (1.94 Å) and weakly interacting with the third one of another layer (2.33 Å). The Mo–O bonding was characterized previously by the electron density-difference maps (deformation density), [10] as well as by the quantum-chemical bond-order indices originating from various approaches; [7–10, 25] the electronic properties of the three oxygen sites on the (010) and (100) surfaces were

This article is dedicated to Prof. Małgorzata Witko.

M. P. Mitoraj · A. Michalak (✉)
Department of Theoretical Chemistry, Faculty of Chemistry, Jagiellonian University, R.Ingardena 3, 30-060 Krakow, Poland
e-mail: michalak@chemia.uj.edu.pl

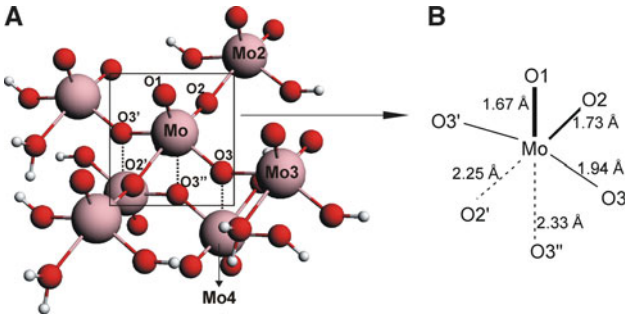


**Fig. 1** Asymmetry in molybdenum–oxygen bonding in the $MoO_3$ crystal structure: the $Mo_7O_{30}H_{18}$ cluster used for modeling the (010) surface of $MoO_3$ (**a**), and the Mo–O distances (**b**; in Å)

characterized, and the oxygen-vacancy formation energies were determined [7–10].

The asymmetry in Mo–O bonds in the $MoO_3$ structure can serve as testing example for new theoretical methods for characterizing chemical bonding. In the present account we will describe the Mo–O bonding in the $Mo_7O_{30}H_{18}$ cluster using the recently developed extended transition state–natural orbitals for chemical valence (ETS–NOCV) approach [26] based on NOCV [27, 28] and the Ziegler–Rauk bond-energy partitioning (ETS) [29]. This approach was successfully applied in characterizing various types of chemical bonds in inorganic and organic compounds, involving donor–acceptor, ionic and covalent bonds as well as relatively weak interactions (hydrogen bonds, agostic bonds) [26, 30–32]. The main advantage of the NOCV-based approach is that it allows one to separate the contributions to the deformation density originating from different components of the bond ($\sigma$-, $\pi$-, $\delta$-), providing the corresponding charge-flow and energy estimates [26–28]. In this article, the ETS–NOCV method is used for the first time to characterize bonding in transition-metal oxide systems, for which the $\sigma$- and $\pi$-components of the metal–oxygen bond has not been explicitly discussed yet.

## Computational details and models

All the DFT calculations presented here were based on the Amsterdam density functional (ADF 2009.01) program [33–37] in which ETS–NOCV scheme was implemented [26]. The Becke–Perdew exchange–correlation functional [33, 34] was applied (BP86). A standard triple-zeta STO basis containing one set of polarization functions (TZP) was adopted for molybdenum, whereas for hydrogen and oxygen, standard double-zeta STO with one set of polarization functions (DZP) were considered. The 1*s* electrons of oxygen as well as 1*s*–3*d* electrons of molybdenum were treated as a frozen core. Relativistic effects for Mo atom were included at ZORA level of approximation as implemented in ADF 2009.01 program. The contours of deformation densities were plotted based on ADF-GUI interface [38].

The bond-analysis performed here is based on the ETS-NOCV approach which is a combination of the ETS [29, 39] bond-energy decomposition with the analysis of the NOCV scheme [26, 27].

The NOCV have been derived from the Nalewajski–Mrozek valence theory [40–45] as eigenvectors that diagonalize the deformation density matrix. It was shown that the pairs of the natural orbitals for chemical valence ($\psi_{-k}$, $\psi_k$, corresponding to eigenvalues $-v_k$ and $v_k$) decompose the differential density $\Delta\rho$ into NOCV-contributions ($\Delta\rho_k$):

$$\Delta\rho(r) = \sum_{k=1}^{M/2} v_k[-\psi_{-k}^2(r) + \psi_k^2(r)] = \sum_{k=1}^{M/2} \Delta\rho_k(r) \qquad (1)$$

where $M$ stands for the number of basis functions. Visual inspection of deformation density plots ($\Delta\rho_k$) helps to attribute symmetry and the direction of the charge- flow. In addition these pictures are enriched by providing charge ($\Delta q_k = |v_k|$) estimations for each charge-flow channel $\Delta\rho_k$. The corresponding energy estimation ($k$-th channel orbital interaction energy) is given by: [26]

$$\Delta E_{\text{orb}}^k = v_k[-F_{-k,-k}^{TS} + F_{k,k}^{TS}] \qquad (2)$$

where $F_{i,i}^{TS}$ are diagonal Kohn–Sham matrix elements defined over NOCV with respect to the transition state density (at the midpoint between density of the molecule and the sum of fragment densities); for further details see Ref. [26].

The ETS–NOCV analysis for Mo–O1, Mo–O2, and Mo–O3 bonds in the $Mo_7O_{30}H_{18}$ cluster modeling the (010) surface of MoO3 was performed by dividing the cluster into two closed-shell fragments: the first fragment containing corresponding oxygen ion $[O1]^{2-}$, $[O2]^{2-}$ or $[O3]^{2-}$, and the second comprising the rest of the cluster (with charge 2+). It should be emphasized here that the choice of the fragments is an arbitrary element of the ETS–NOCV approach. In principle, one could consider atomic (neutral) or ionic (charged) fragments.

## Results and discussion

As it has been already mentioned in introduction [7, 24] there exist three non-equivalent types of oxygen atoms (O1, O2, and O3) in $MoO_3$ crystal characterized by different Mo–O distances, see Fig. 1.

Let us first discuss leading deformation density contributions and the corresponding energies (see Eqs. 1 and 2) originating from ETS–NOCV scheme that characterize the interaction between terminal oxygen ion, $[O1]^{2-}$ and the rest

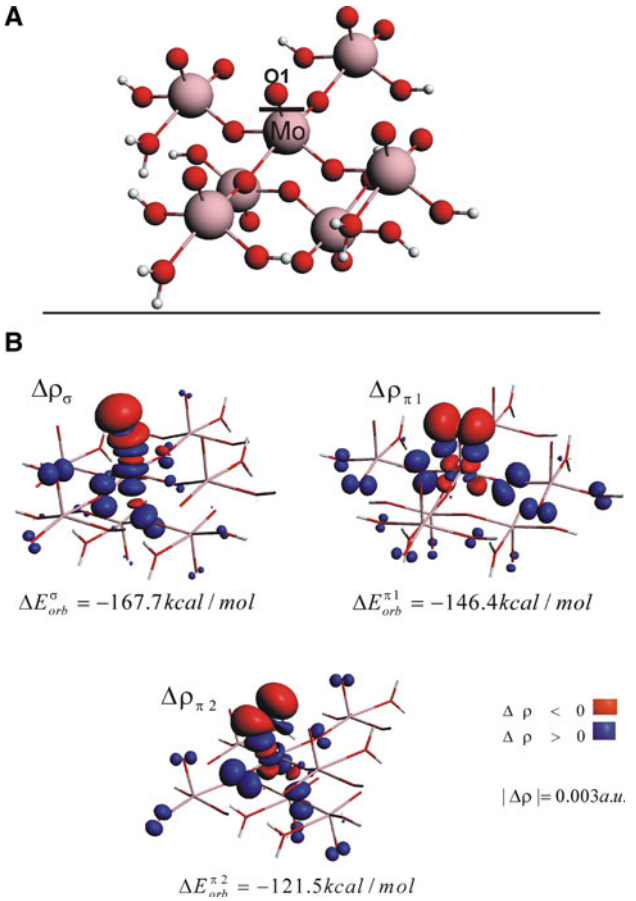


**Fig. 2** Mo–O1 bonding. In **a** *black line* crossing Mo–O1 bond indicates division of cluster into two fragments that were used in ETS–NOCV analysis. Contours of deformation density contributions $\Delta\rho_\sigma$, $\Delta\rho_{\pi 1}$, $\Delta\rho_{\pi 2}$ together with the corresponding energies $\Delta E^{\sigma}_{\mathrm{orb}}$, $\Delta E^{\pi 1}_{\mathrm{orb}}$, $\Delta E^{\pi 2}_{\mathrm{orb}}$ describing the interaction between oxygen $(O1)^{2-}$ and the rest of the cluster (**b**). The contour values are $\pm 0.003 a.u$

of the cluster. It is clear from part B of Fig. 2 that three components are of the vital importance for Mo–O1 bonding, one $\sigma$-contribution, $\Delta\rho_\sigma$, with the corresponding stabilization $\Delta E^{\sigma}_{\mathrm{orb}} = -167.7$ kcal/mol, and the two $\pi$-components, $\Delta\rho_{\pi 1}$, $\Delta\rho_{\pi 2}$, characterized by $\Delta E^{\pi 1}_{\mathrm{orb}} = -146.4$ kcal/mol and $\Delta E^{\pi 2}_{\mathrm{orb}} = -121.5$ kcal/mol, respectively. Total stabilization energy from both Mo–O1 $\pi$-terms dominates over $\sigma$-bonding and $\pi/\sigma$ ratio is ca. 1.7. Similar trend was found using charge estimation of these bonding channels, see Table 1. It is noteworthy that $\sigma$-contribution is not only based on the charge transfer from $2p$ orbital of oxygen to molybdenum and the neighboring oxygen atoms (ionic contribution) but as well as to the bonding region of Mo–O1 (covalent term). Similar conclusion on the presence of ionic and covalent terms is true for $\pi$-contributions, see Fig. 2. The existence of both components is in agreement with the previous studies [10, 46, 47].

Considering the bonding between asymmetric oxygen $[O2]^{2-}$ and the remaining part of the cluster one can see

**Table 1** ETS–NOCV energy decomposition results describing the interaction between oxygen sites $[O1]^{2-}$, $[O2]^{2-}$, $[O3]^{2-}$ and the rest of the cluster

| ETS–NOCV[a,b] | O1 | O2 | O3 |
|---|---|---|---|
| $\Delta E^{\sigma}_{\mathrm{orb}}$ | −167.7 | −130.6 | −107.1 |
| $\Delta E^{\pi 1}_{\mathrm{orb}}$ | −146.4 | −125.6 | −56.1 |
| $\Delta E^{\pi 2}_{\mathrm{orb}}$ | −121.5 | −74.5 | −61.9 |
| $\Delta E^{\sigma+\pi}_{\mathrm{orb}}$ | −435,6 | −330,7 | −225,1 |
| NOCV | | | |
| $\Delta q^{\sigma}$ | 1.00 | 0.80 | 0.74 |
| $\Delta q^{\pi 1}$ | 1.05 | 1.05 | 0.60 |
| $\Delta q^{\pi 2}$ | 0.89 | 0.70 | 0.54 |

In addition charge estimations ($\Delta q_i$) of bonding contributions are presented

[a] $\Delta E^{\sigma+\pi}_{\mathrm{orb}} = \Delta E^{\sigma}_{\mathrm{orb}} + \Delta E^{\pi 1}_{\mathrm{orb}} + \Delta E^{\pi 2}_{\mathrm{orb}}$, units are in kcal/mol

[b] For fragmentation details, see **a** in Figs. 2, 3 and 4

from B of Fig. 3 that three dominant deformation density channels are also important, one $\sigma$–($\Delta\rho_\sigma$) and two $\pi$-bonds ($\Delta\rho_{\pi 1}$, $\Delta\rho_{\pi 2}$). It is necessary to point out that they are localized in the Mo–O2 bonding region and nearly no electronic coupling with the adjacent molybdenum atom (Mo2; $R_{\mathrm{Mo2–O2}} = 2.25$ A) is observed, see Fig. 3b. Qualitatively, they exhibit similar features as in the case of Mo–O1 connection. However, quantitatively these contributions appeared to be notably weaker, $\Delta E^{\sigma}_{\mathrm{orb}}$ is lower (in absolute term) by 31.7 kcal/mol, $\Delta E^{\pi 1}_{\mathrm{orb}}$ by 20.8 and $\Delta E^{\pi 2}_{\mathrm{orb}}$ by 40.7 kcal/mol. This is due to a weaker overlap between the orbitals participating in Mo–O2 bonding resulting from the Mo–O2 bond elongation, compared to Mo–O1. Lengthening of the Mo–O2 bond can be in turn related to the electrostatic attraction between O2 and the neighboring Mo2 and/or to the fact that the same $d_\pi$ orbitals participate in the formation of the $\pi$-component of the Mo–O2 and Mo–O1 bonds or the Mo–O2 and Mo–O3 bonds. The ratio characterizing relative energetic strength of $\pi/\sigma$ components becomes lower (as compared to Mo–O1 connection) and is equal to 1.53. Similar trend on weaker electronic stabilization of Mo–O2 bond is true when analyzing the charge estimations of deformation density channels ($\Delta q^{\sigma}$, $\Delta q^{\pi 1}$, $\Delta q^{\pi 2}$), see Table 1. As it can be seen the strengths of $\sigma(m\Delta q^{\sigma})$ and total $\pi$-contribution ($\Delta q^{\pi 1} + \Delta q^{\pi 2}$) are lower in the case of Mo–O2 connection. It should be finally noticed that weaker strength of these components (obtained consistently on the basis of energetic and charge criterions) make the Mo–O2 bond longer as compared to Mo–O1, by 0.05 Å (see Fig. 1).

Finally, let us characterize the interaction between oxygen, $[O3]^{2-}$, and the rest of the cluster. In this case three deformation density channels, presented in part B of Fig. 4, characterize symmetrical formation of both Mo–O3 and O3–Mo3 connections. Such charge transfer is

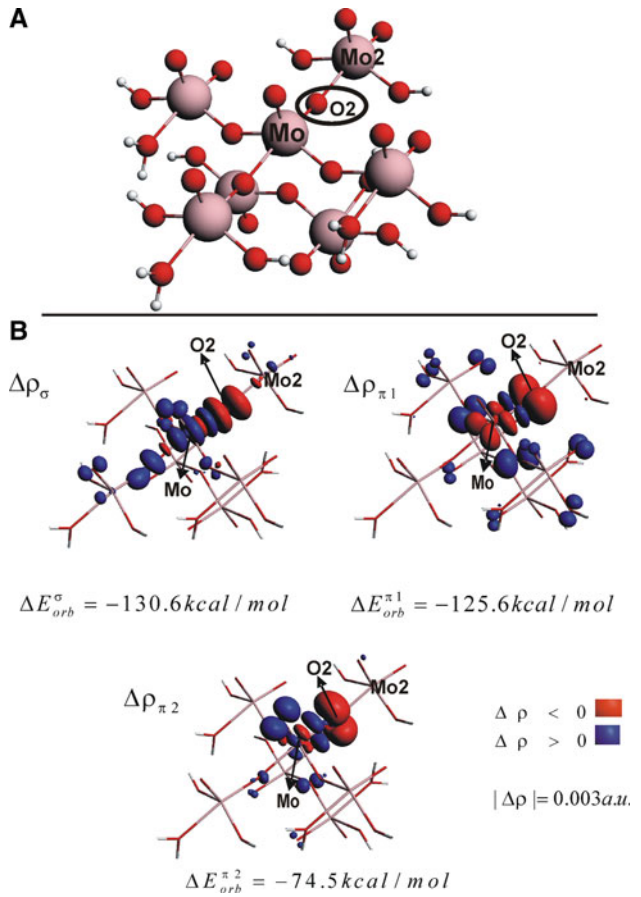


**Fig. 3** Mo–O2 bonding. Two fragments used in the ETS–NOCV analysis (**a**). Contours of deformation density contributions $\Delta\rho_\sigma$, $\Delta\rho_{\pi 1}$, $\Delta\rho_{\pi 2}$ together with the corresponding energies $\Delta E^{\sigma}_{\text{orb}}$, $\Delta E^{\pi 1}_{\text{orb}}$, $\Delta E^{\pi 2}_{\text{orb}}$ describing the interaction between oxygen $(O2)^{2-}$ and the rest of the cluster (**b**). The contour values are ±0.003 a.u.

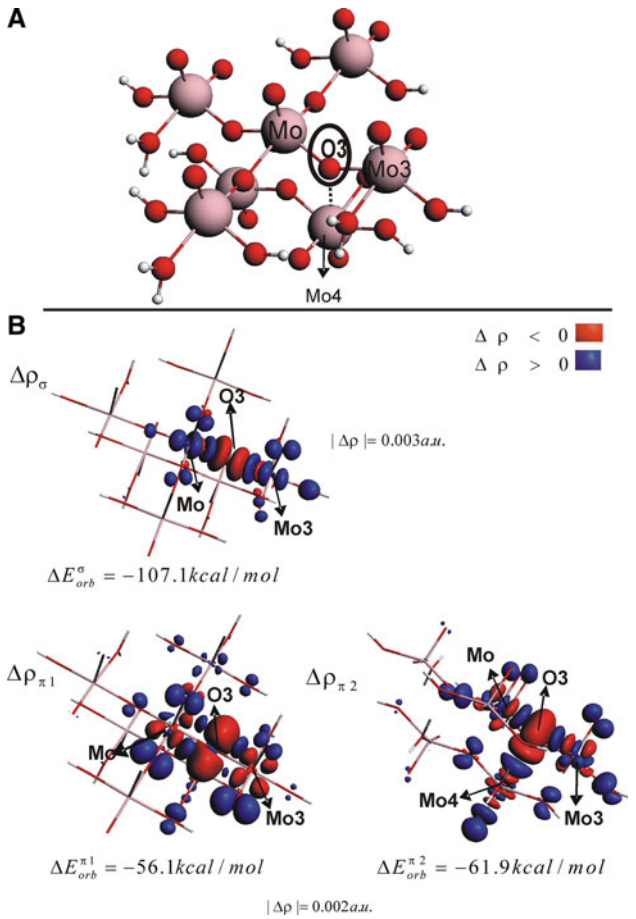


**Fig. 4** Mo–O3 bonding. The fragments used in the ETS–NOCV analysis (**a**). Contours of deformation density contributions $\Delta\rho_\sigma$, $\Delta\rho_{\pi 1}$, $\Delta\rho_{\pi 2}$ together with the corresponding energies $\Delta E^{\sigma}_{\text{orb}}$, $\Delta E^{\pi 1}_{\text{orb}}$, $\Delta E^{\pi 2}_{\text{orb}}$ describing the interaction between oxygen $(O3)^{2-}$ and the rest of the cluster (**b**). The contour values are ±0.003 a.u. for $\sigma$- contribution, whereas ±0.002 a.u. values were used for $\pi$-bonding (magnified contour, in order to improve clarity)

consistent with the fact that O3 is symmetrically bonded to the neighboring molybdenum atoms, with both Mo–O3 and O3–Mo3 distances equal to 1.94 Å. In addition, it is worth pointing out that the contour of $\Delta\rho_{\pi 2}$ partly characterize the coupling of O3 with the Mo4 atom that belongs to underlying sublayer.

Considering the energetic measures of the O3–Mo and O3–Mo3 bonds, one can observe that total strength of both $\sigma$-bonds is $\Delta E^{\sigma}_{\text{orb}} = -107.1$ kcal/mol, what gives −53.55 kcal/mol per each of $\sigma$(O3–$X$) connection ($X$ = Mo, Mo3), see Fig. 4 and Table 1. The strengths of $\pi$-contributions are −28.05 kcal/mol and −30.95 kcal/mol, for each $\pi$-component, $\pi 1$(O3–$X$) and $\pi 2$(O3–$X$), respectively. Slightly stronger contribution characterized by $\Delta\rho_{\pi 2}$ (as compared to $\Delta\rho_{\pi 1}$) is related to the coupling of O3 with Mo4 site belonging to underlying sublayer—clearly, the lobe of oxygen 2$p$ orbital overlaps with $d_{z2}$ orbital of Mo4 leading to the charge transfer to O3–Mo4 bonding region, see Fig. 4. It is interesting to observe that such electronic coupling is evidently visible despite relatively large O3–Mo4 distance (2.33 Å), whereas for O2–Mo2 with the distance 2.25 Å no such coupling was found (see Fig. 3). Finally, in the case of O3 bonding, $\pi$-component is of the same importance as $\sigma$-connection ($\pi/\sigma$ ratio is 1.1).

It is worth commenting at this point on the possible influence of the basis set and the relativistic correction on the ETS–NOCV results presented here. In Table 2, we compare the results calculated with and without the ZORA relativistic correction and with TZP and TZ2P basis set for Mo–O1 bond. The results clearly show that the effect of both, the basis set as well as relativistic correction (<2 kcal/mol; i.e. 1–2 %) is not important for the qualitative conclusions from the present study; these effects are negligible comparing to the presented changes in the orbital interaction energy contributions for different Mo–O bonds (15–40 %).

Summarizing the ETS–NOCV results, we would like to emphasize that in this approach the bond between the

**Table 2** Influence of the basis set and relativistic correction on the orbital interaction energy contribution calculated for Mo–O1 bond

| Orbital interaction energy terms (Mo–O1 bond) | TZP/ ZORA | TZ2P/ ZORA | TZP/ no[a] |
|---|---|---|---|
| $\Delta E^{\sigma}_{\mathrm{orb}}$ | −167.7 | −169.1 | −169.5 |
| $\Delta E^{\pi 1}_{\mathrm{orb}}$ | −146.4 | −147.3 | −147.0 |
| $\Delta E^{\pi 2}_{\mathrm{orb}}$ | −121.5 | −123.6 | −122.8 |

[a] No relativistic correction

molecular *fragments* is characterized and the choice of the interacting fragments can be arbitrary. While in many cases of molecular systems the choice of fragments is very natural, in the case of the transition-metal oxides one can consider the *atomic* or *ionic fragments* (i.e., neutral O or the $O^{2-}$ anion), as the metal–oxygen bonds exhibit partly covalent and partly ionic character. As an obvious consequence, the energetic estimates of the *i*-th charge-flow channel, $\Delta E^{i}_{\mathrm{orb}}$, depend on the choice of the fragments, and can be used only as a qualitative measure of relative importance of the bond-components. In the present study we used ionic fragments. The results clearly show that increase in Mo–O distances, from 1.68 Å (for O1), through 1.73 Å (for O2), up to 1.94 Å (for O3) is directly related to decrease in the strength of both $\sigma$- and two $\pi$-contributions of Mo–O bond (see part A of Fig. 5). It should also be pointed out that the total strength of $\sigma$- and $\pi$-contributions (estimated by the sum $\Delta E^{\sigma}_{\mathrm{orb}} + \Delta E^{\pi 1}_{\mathrm{orb}} + \Delta E^{\pi 2}_{\mathrm{orb}}$) correlate very well ($R^2 = 0.98$) with the vacancy formation energies calculated by Tokarz-Sobieraj et al. [7], corresponding to the interaction of *atomic* oxygen with the rest of the cluster; this is illustrated in Fig. 5b. This very good correlation shows that both, ionic and atomic reference frames lead to a similar, qualitative picture of bonding. This a posteriori justifies use of *ionic* fragments in ETS–NOCV analysis presented here.

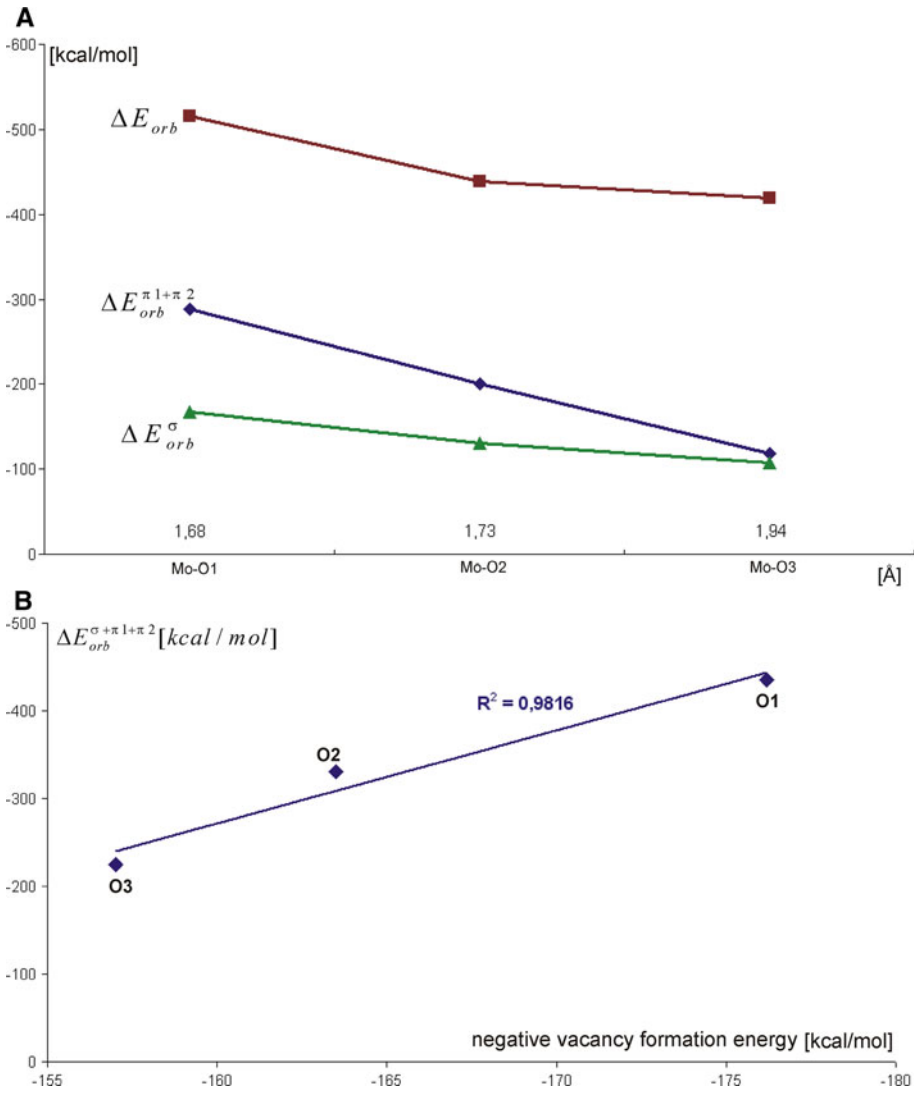


**Fig. 5** Qualitative correlation between Mo–O distances (O1, O2, O3) and the total orbital interaction term together with the strength of individual $\sigma$- and total $\pi$-contributions obtained from ETS–NOCV scheme (**a**). In addition, the correlation between total strength of all bonding contributions ($\Delta E^{\sigma+\pi 1+\pi 2}_{\mathrm{orb}}$) and negative vacancy formation energies obtained by Tokarz-Sobieraj et al. [7] were presented in **b**

## Concluding remarks

In the present study, we have verified applicability of ETS–NOCV scheme in a description of bonding of three inequivalent oxygen sites (O1, O2, O2) in the cluster modeling (010) surface of $MoO_3$. We have considered oxygen atoms that are characterized by different Mo–O distances, 1.68 Å (for O1), 1.73 Å (for O2), and 1.94 Å (for O3).

We have found based on ETS–NOCV scheme that such systematic increase in the Mo–O distances is directly related to decrease in the strength of both $\sigma$- and two $\pi$-contributions of Mo–O bond. Qualitatively, these contributions appeared to show both ionic (the charge transfer from 2*p* orbital of oxygen to molybdenum) and the covalent components (charge accumulation in the Mo–O region). Moreover, it is gratifying to see that ETS–NOCV appeared to be useful not only in a description of strong molybdenum–oxygen connections, but also the weak coupling, for example between O2 and Mo4 could be detected (see $\Delta\rho_{\pi 2}$ in Fig. 4). It should be finally pointed out that the trend in total strength of $\sigma$- and two $\pi$-contributions ($\Delta E_{\mathrm{orb}}^{\sigma+\pi}$) correlate very well with the vacancy formation energies calculated by Tokarz-Sobieraj et al. [7].

**Acknowledgments** Mariusz P. Mitoraj greatly acknowledge the financial supports from the Foundation for Polish Science ("START" scholarship) as well as from Polish Ministry of Science and Higher Education ("Outstanding Young Researchers" scholarship). This study was also supported by a research grant from the Ministry of Science and Higher Education in Poland (N N204 198040).



## References

1. Haber J, Witko M (1981) Acc Chem Res 14:1
2. Witko M, Haber J (1980) J Mol Catal 9:399
3. Slater JC, Johnson KH (1974) Phys Today 27:34
4. Beran S, Zahradnik R (1977) Kinet Catal 18:359
5. Beran S, Czarski P, Gobza N, Pancir I, Polak R, Slaneria Z, Zahradnik R (1978) Usp Khim 11:1905
6. Baetzold RG (1976) Adv Catal 25:1
7. Tokarz-Sobieraj R, Hermann K, Witko M, Blume A, Mestl G, Schlögl R (2001) Surf Sci 489:107
8. Hermann K, Witko M, Michalak A (1999) Catal Today 50:567
9. Hermann K, Michalak A, Witko M (1996) Catal Today 32:321
10. Michalak A, Hermann K, Witko M (1996) Surf Sci 366:323
11. Tokarz-Sobieraj R, Gryboś R, Witko M (2011) Appl Catal A 391:137
12. Słoczyński J, Grabowski R, Kozłowska A, Tokarz-Sobieraj R, Witko M (2007) J Mol Catal A 277:27
13. Tokarz-Sobieraj R, Witko M, Gryboś R (2005) Catal Today 99:241
14. Witko M, Tokarz-Sobieraj R (2004) Catal Today 91–92:171
15. Czekaj I, Hermann K, Witko M (2003) Surf Sci 525:33
16. Haras A, Duarte HA, Salahub DR, Witko M (2002) Surf Sci 513:367
17. Witko M, Tokarz-Sobieraj R, Haber J, Hermann K (2001) J Mol Catal A 166:59
18. Witko M, Hermann K, Tokarz-Sobieraj R (1999) Catal Today 50:553
19. Hermann K, Witkoq M, Druzinic R, Chakrabarti A, Tepper B, Elsner M, Gorschlüter A, Kuhlenbeck H, Freund HJ (1999) J Electron Spectrosc Relat Phenom 98-99:245
20. Michalak A, Witko M, Hermann K (1997) Surf Sci 375:385
21. Haber J, Witko M (1995) Catal Today 23:311
22. Kung HK (1989) Transition-metal oxides: surface chemistry and catalysis. In: Delmon B, Yates JT (eds) Studies in surface science and catalysis, vol 45. Elsevier, Amsterdam
23. Krylov OV, Kiselev VF (1989) In: Ertl G, Gomer R (eds) Adsorption and catalysis on transition-metals and their oxides. Springer, New York
24. Kihlborg L (1963) Arkiv Kemi 21:357
25. Michalak A, De Kock R, Ziegler T (2008) J Phys Chem A 112:7256
26. Mitoraj M, Michalak A, Ziegler T (2009) J Chem Theory Comput 5(4):962
27. Mitoraj M, Michalak A (2007) J Mol Model 13:347–355
28. Michalak A, Mitoraj M, Ziegler T (2008) J Phys Chem A 112:1933
29. Ziegler T, Rauk A (1977) Theor Chim Acta 46:1
30. Broclawik E, Załucka J, Kozyra P, Mitoraj M, Datka J (2010) J Phys Chem C 114:9808
31. Rejmak P, Mitoraj M, Broclawik E (2010) Phys Chem Chem Phys 12:2321
32. Broclawik E, Mitoraj M, Rejmak P, Michalak A (2010) In: Frank Columbus (ed) Handbook of inorganic chemistry research. Nova Publisher, New York, pp 361–383. ISBN: 978-1-61668-010-7
33. Baerends EJ, Autschbach J, Bashford D, Berger JA, Brces A, Bickelhaupt FM, Bo C, de Boeij PL, Boerrigter PM, Cavallo L, Chong DP, Deng L, Dickson RM, Ellis DE, van Faassen M, Fan L, Fischer TH, Fonseca Guerra C, Giammona A, Ghysels A, van Gisbergen SJA, Gtz AW, Groeneveld JA, Gritsenko OV, Gr ning M, Harris FE, van den Hoek P, Jacob CR, Jacobsen H, Jensen L, Kadantsev ES, van Kessel G, Klooster R, Kootstra F, Krykunov MV, van Lenthe E, Louwen JN, McCormack DA, Michalak A, Mitoraj M, Neugebauer J, Nicu VP, Noodleman L, Osinga VP, Patchkovskii S, Philipsen PHT, Post D, Pye CC, Ravenek W, Rodrguez JI, Romaniello P, Ros P, Schipper PRT, Schreckenbach G, Seth M, Snijders JG, Sol M, Swart M, Swerhone D, te Velde G, Vernooijs P, Versluis L, Visscher L, Visser O, Wang F, Wesolowski TA, van Wezenbeek EM, Wiesenekker G, Wolff SK, Woo TK, Yakovlev AL, Ziegler T (2009) ADF 2009. 01. SCM, Amsterdam
34. te Velde G, Bickelhaupt FM, Baerends EJ, Fonseca Guerra C, van Gisbergen SJA, Snijders JG, Ziegler T (2001) J Comput Chem 22:931 and ref therein
35. Baerends EJ, Ellis DE, Ros P (1973) Chem Phys 2:41
36. Boerrigter PM, te Velde G, Baerends EJ (1988) Int J Quantum Chem 33:87
37. Fonesca Geurra C, Visser O, Snijders JG, te Velde G, Baerends EJ (1995) In: Clementi E, Corongiu G (eds) Methods and techniques in computational chemistry METACC-9. STEF, Cagliari, p 303
38. Visser O, Leyronnas P, van Zeist W-J, Lupki M ADF-GUI 2009.01, SCM, Amsterdam, The Netherlands, http://www.scm.com
39. Bickelhaupt FM, Baerends EJ (2000) Reviews in computational chemistry. In: Lipkowitz KB, Boyd DB (eds) Kohn-Sham density functional theory: predicting and understanding chemistry, vol 15. VCH, New-York, p 1

40. Nalewajski RF, Köster AM, Jug K (1993) Theor Chim Acta 85:463
41. Nalewajski RF, Mrozek J (1994) Int J Quantum Chem 51:187
42. Nalewajski RF, Mrozek J, Formosinho SJ, Varandas AJC (1994) Int J Quantum Chem 52:1153
43. Nalewajski RF, Mrozek J, Mazur G (1996) Can J Chem 74:1121
44. Nalewajski RF, Mrozek J, Michalak A (1997) Int J Quantum Chem 61:589
45. Nalewajski RF, Mrozek J, Michalak A (1998) Pol J Chem 72:1779
46. Papakondylis A, Sautet P (1996) J Phys Chem 100:10681
47. Chen M, Waghmare M, Friend CM, Kaxiras E (1998) J Chem Phys 109:6854